Article

(Tetrafluorovinylphenyl)carbazole as a Multifunctional Material for OLED Applications

Khrystyna Ivaniuk, Pavlo Stakhira, Iryna Yaremchuk, Stepan Kutsiy, Tetiana Bulavinets, Dmytro Volyniuk, Ivan Klymenko, Galyna Sych, Nataliya Karaush-Karmazin, Amjad Ali, Aliaksei Vaitusionak, Sergei V. Kostjuk, Juozas Vidas Grazulevicius,* and Glib V. Baryshnikov*

Cite This: *ACS Appl. Electron. Mater.* 2023, 5, 2156−2168

Read Online

ACCESS | Metrics & More | Article Recommendations | Supporting Information

ABSTRACT: The multifunctional materials for application in organic light-emitting devices (OLEDs) based on a single structural motif are very desired but quite rare species. Such structures allow simplifying the chemical variety within OLED heterostructures and thus reducing their cost, manufacturing time, and logistic efforts. In this paper, we report the 9-(2,3,5,6-tetrafluoro-4-vinylphenyl)carbazole molecule (Cz4FS) utilized as a fluorescent emitter, host material for quantum dot based OLEDs (QLEDs), acceptor part of the exciplex active layer, and monomer that can be used for the preparation of emissive polymers and copolymers. The external quantum efficiency (EQE) of the corresponding fluorescent OLED based on a Cz4FS single emitter doped into a 1,3-bis(carbazol-9-yl)benzene matrix is 4.2%, which is close to the theoretical limit and maximum brightness at the level of 3600 cd/m². An OLED based on exciplex emission obtained utilizing Cz4FS as an acceptor demonstrates higher efficiency (5.3%) and much higher brightness near 25 000 cd/m². A QLED based on Cz4FS as a host for CdSeS/ZnS core−shell quantum dots demonstrates excellent energy transfer from the Cz4FS matrix that results in a clear spectrum of quantum dots with an EQE of 2.3%, maximum of 19 000 cd/m², and narrow spectral distribution. An OLED based on a Cz4FS-based polymer and copolymer demonstrates not extraordinary efficiency but low-efficiency roll-off in a wide range of current densities.

KEYWORDS: *exciplex, OLED, fluorescence, polymer, quantum dots, charge transfer*
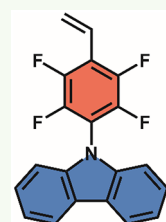
emitter
host matrix
exciplex-forming
polymerization
copolymerization

INTRODUCTION

Organic light-emitting diodes (OLEDs) have great potential in the fields of modern displays and organic lighting due to their low energy consumption, flexibility, high color quality, and potentially low cost.[1−5] OLED technology has been successfully commercialized due to the significant advances in the synthesis and research of organic low-molecular-weight and polymer semiconductors, as well as due to advances in the design and engineering of efficient device architectures.[6−8] Many types of emissive materials including fluorescent,[9,10] thermally activated delayed fluorescent (TADF),[11,12] phosphorescent,[13−15] organic radical, and radical polymer[16,17] emitters have been utilized as active materials in OLEDs due to their numerous advantages such as high electroluminescence quantum yield through high internal quantum efficiency, long-term stability, high conductivity, and charge carrier mobility. However, all these factors require a chemical variety with respect to the structure of the emitters, while a unified structural motif is very desirable for achieving multifunctional OLED materials.

It should be noted that the problem of development of highly efficient and stable deep blue emitters as one of the three color primaries (RGB) remains urgent as a part of the manufacturing of white OLEDs and full-color displays.[18,19] An ideal blue-light-emitting material would have Commission Internationale d'Eclairage (CIE) coordinates of (0.14, 0.08), as specified in the National Television System Committee (NTSC) standard. However, now they are far from satisfactory for most blue emitters.[20] The deep blue color is defined arbitrarily as having a blue electroluminescent emission with (CIE) x, y coordinates of $x \sim 0.15$ and $y < 0.15$.[21] Until now, there have only been a few reported deep blue emitters and the corresponding highly efficient and stable OLEDs with satisfactory chromaticity coordinates.[22] The problem is both in the wide band gap of high-energy blue OLEDs and in the often occurring unbalance in electron and hole mobilities due to the mismatch in the positions of the energy levels in the organic light-emitting heterostructures.[23] Moreover, the short-wavelength deep blue emission corresponding to the energy near 3.10 eV significantly increases the probability of molecular degradation[24] by light reabsorption, which adversely affects the long-term stability of blue OLED. A comprehensive solution to
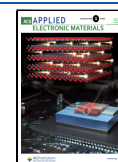
these problems can be reached by the development of high-performance blue emitters with donor–acceptor (D–A) structures with the narrow spectral distribution of emission and small full width at half-maximum (fwhm) and capability of transporting both electrons and holes. Such a strategy can promote fluorescence efficiency, but can cause a bathochromic effect of the emission spectra.

Deep blue D–A molecules can be synthesized by rational design and proper selection of electron-donating and electron-accepting fragments. Introduction of strongly electronegative fluorine or fluorine-containing groups in an aromatic polymer core is a useful strategy in order to enhance electron-withdrawing properties and adjust the electron affinity value of materials as well as allows modification of molecular orientation and improvement of electron-transporting properties.[25−28] Moreover, the trade-off between the number of incorporated fluorine atoms/fluorinated groups and donor–acceptor strength in the semiconducting material is a key toward high-performance blue-OLEDs.[29,30] Organic compounds designed for electroluminescent devices have to possess strong emission in the solid state. One of the approaches for achieving high fluorescence efficiency and avoiding aggregation-caused quenching in the solid state is the utilization of aggregation-induced emission (AIE), which enables the radiative channels for the decay of excited states[31,32] and disables nonradiative processes. AIE systems usually exhibit efficient solid-state emission by suppressing concentration quenching and exciton annihilation. In contrast to conventional fluorophores, AIE-active fluorophores are almost nonluminescent in dilute solutions, while becoming highly luminescent upon molecular aggregation. One of the reasons for the AIE phenomenon is the restriction of nonradiative vibrational relaxation processes in the solid state due to the restriction of the intramolecular motions of molecular fragments.[33,34] In this work, we studied the luminescence mechanisms taking place in OLEDs and quantum dot based OLEDs (QLEDs) based on AIE-active D–A compound 9-(2,3,5,6-tetrafluoro-4-vinylphenyl)-9H-carbazole (Cz4FS)[35,36] consisting of an electron-deficient tetrafluorobenzene fragment and electron-donating carbazole unit in the *para*-position of polytetrafluorostyrene.

The efficiency of energy transfer from the host 1,3-bis(carbazol-9-yl)benzene (mCP) to the emitter (Cz4FS) is discussed in this report. Comparing the absorption spectrum of the solid film of Cz4FS and the photoluminescence spectrum (fwhm is 30−40 nm at the emission maximum $\lambda_{max} = 490 \pm 5$ nm) of CdSeS/ZnS QD, we observed well-overlapped guest absorption and host emission spectra, which imply that efficient Forster resonance energy transfer (FRET) may occur once CdSeS/ZnS alloyed quantum dots are doped in Cz4FS. We thus found the possibility to use Cz4FS as the host component for guest CdSeS/ZnS core–shell quantum dots[37] in the fabrication of the corresponding QLEDs.

■ EXPERIMENTAL SECTION

Materials and Instrumentation. The 9-(2,3,5,6-tetrafluoro-4-vinylphenyl)-9H-carbazole (Cz4FS), related polymer (P1), and copolymer of Cz4FS with 9-(4-vinylphenyl)carbazole (LRC-13) containing 13 mol % of the later monomer units were synthesized as described in refs 35 and 36. The molar percentage ratio of monomer units (9-(4-vinylphenyl)carbazole (M1) and 9-(2,3,5,6-tetrafluoro-4-vinylphenyl)carbazole (M2)) in the LRC-13 copolymer was previously calculated by the integration of the NMR spectra of the copolymer.[36] Their structures are presented in Scheme 1. All

other chemicals (components of OLEDs) were purchased from Sigma-Aldrich and were used without additional purification.

Scheme 1. Structures of 9-(2,3,5,6-Tetrafluoro-4-vinyl phenyl)-9H-carbazole (Cz4FS), Poly[9-(4-vinylphenyl)carbazole] (P1), and the Copolymer of Cz4FS and 9-(4-Vinylphenyl)carbazole (LRC-13) with the Molar Percentage Ratio of 87:13, Respectively
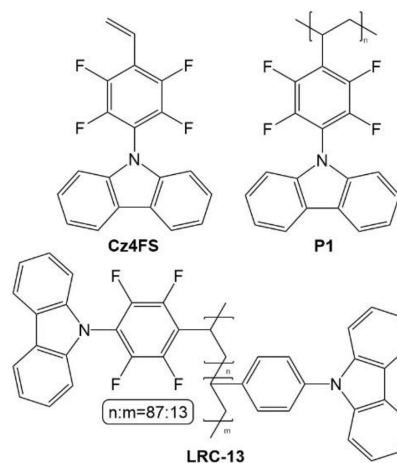
Photoluminescence spectra of the films with different concentrations of Cz4FS in mCP were recorded with the Edinburgh Instruments FLS980 spectrometer and PicoQuant LDH-DC-375 laser (wavelength 374 nm) as the excitation source at room temperature. The photoluminescence quantum yield measurements were performed using an integrated sphere (inner diameter of 120 mm). Electroluminescent devices were fabricated by spin-coating and thermovacuum evaporation methods. The devices were deposited on the glass substrates from Ossila with prepatterned bottom indium tin oxide (ITO) electrodes. First, the layer (CuI) was deposited by centrifugation at 1000 rpm, followed by annealing at the temperature of 50 °C. In the cases of devices A and B, organic functional layers were fabricated by the thermovacuum evaporation method. In the case of devices C and D, the light-emitting layers (Cz4FS:CdSeS/ZnS and P1:LRC-13) were spin-coated, while the other layers (TSPO1/TPBi) were deposited in a vacuum, respectively. During the device fabrications, the vacuum chamber was always kept at the pressure of 2 × 10⁻⁶ mbar. All of the vacuum-evaporated layers were deposited at a rate of 1−2 Å s⁻¹. In the case of devices C and D, light-emitting layers were deposited from toluene solutions (1 mg/mL) of the corresponding compound mixtures. After spin-coating of the light-emitting layer, the samples were thermally annealed at 50 °C for 30 min (in the case of the Cz4FS:CdSeS/ZnS layer) or 90 °C for 40 min (in the case of the P1:LRC-13 layer) using an electric hot plate. The top Ca:Al cathode and vacuum-deposited organic layers were deposited using appropriate shadow masks (also from Ossila). In such cases, four OLED pixels with the size of 4.5 mm² were obtained per one substrate. Furthermore, measurement was made after the creation of the device, in the air without passivation and capsulation. The luminance voltage and current density voltage dependences were measured with brightness, and the semiconductor parameters analyzer (HP 4145A) was measured using a calibrated photodiode. The brightness measurements were done using a calibrated photodiode.[38] The electroluminescence (EL) spectra were recorded with an Ocean Optics USB2000 spectrometer.

For single-crystal X-ray analysis, a single crystal of Cz4FS was grown from acetone solution by the slow diffusion method using cyclohexane as an antisolvent. The crystallographic analysis was performed employing the XtaLAB mini diffractometer (Rigaku) with a graphite-monochromated Mo Kα (λ = 0.71075 Å) X-ray source at room temperature (295 K). The structure of Cz4FS was solved with the ShelXT structure solution program using Intrinsic Phasing and

a)

b)

c)

d)
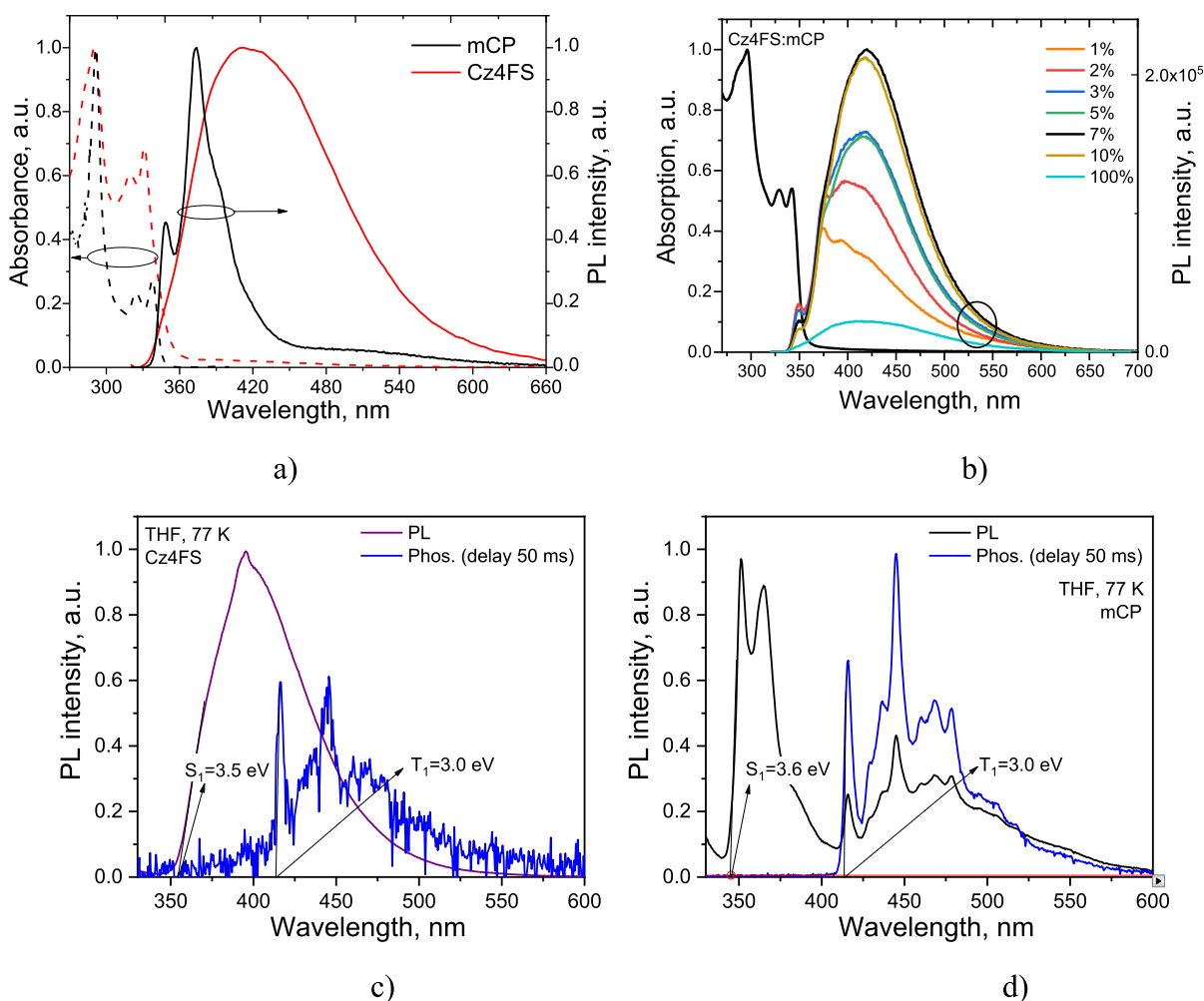
Figure 1. Absorption and photoluminescence spectra of mCP and Cz4FS (a) and their solid-state mixtures Cz4FS:mCP (b) with different concentration of the guest. PL and phosphorescence (Phos.) spectra of THF solutions of Cz4FS (c) and mCP (d) at 77 K (λ_{exc} = 300 nm).

refined with the ShelXL refinement package using least squares minimization. The parameters of its X-ray structure can be deduced using the crystallographic data of Cz4FS deposited in the Cambridge Crystallographic Data Centre with the corresponding CCDC deposition number 2243665.

■ RESULTS AND DISCUSSION

Photophysical Properties. In the first stage, we investigated the photophysical properties of Cz4FS. mCP

Table 1. Photophysical Characteristics for the Host−Guest System of mCP and Cz4FS with Different Concentrations of mCP

|	1% Cz4FS	2% Cz4FS	3% Cz4FS	5% Cz4FS	7% Cz4FS	10% Cz4FS
λ^{PL}, nm			415	415	416	419
PLQY, %	5	6	9	11	15	17

was used as a matrix component to investigate energy transfer efficiency from the host material to the emitter Cz4FS. The selection of the host matrix was due to the low polarity of mCP (ε = 2.84[39]), which does not affect the deep blue emission wavelength of the guest component (Cz4FS).[35] FRET efficiency is highly dependent on the spectral overlap between the absorption of guest Cz4FS and the emission of host mCP
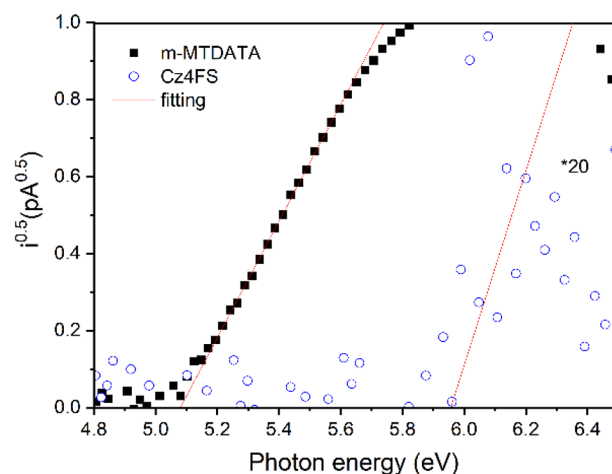
Figure 2. Photoelectron emission spectrum of the solid films of m-MTDATA and Cz4FS.

(Figure 1a).[40] The low-energy absorption band of Cz4FS resulted from the charge transfer between its donor and acceptor units, as it was previously discussed.[35]

Photophysical properties of various emitter concentrations ranging from 1% to 10% in mCP were studied to clarify and evaluate the level of energy transfer in the host−guest system.
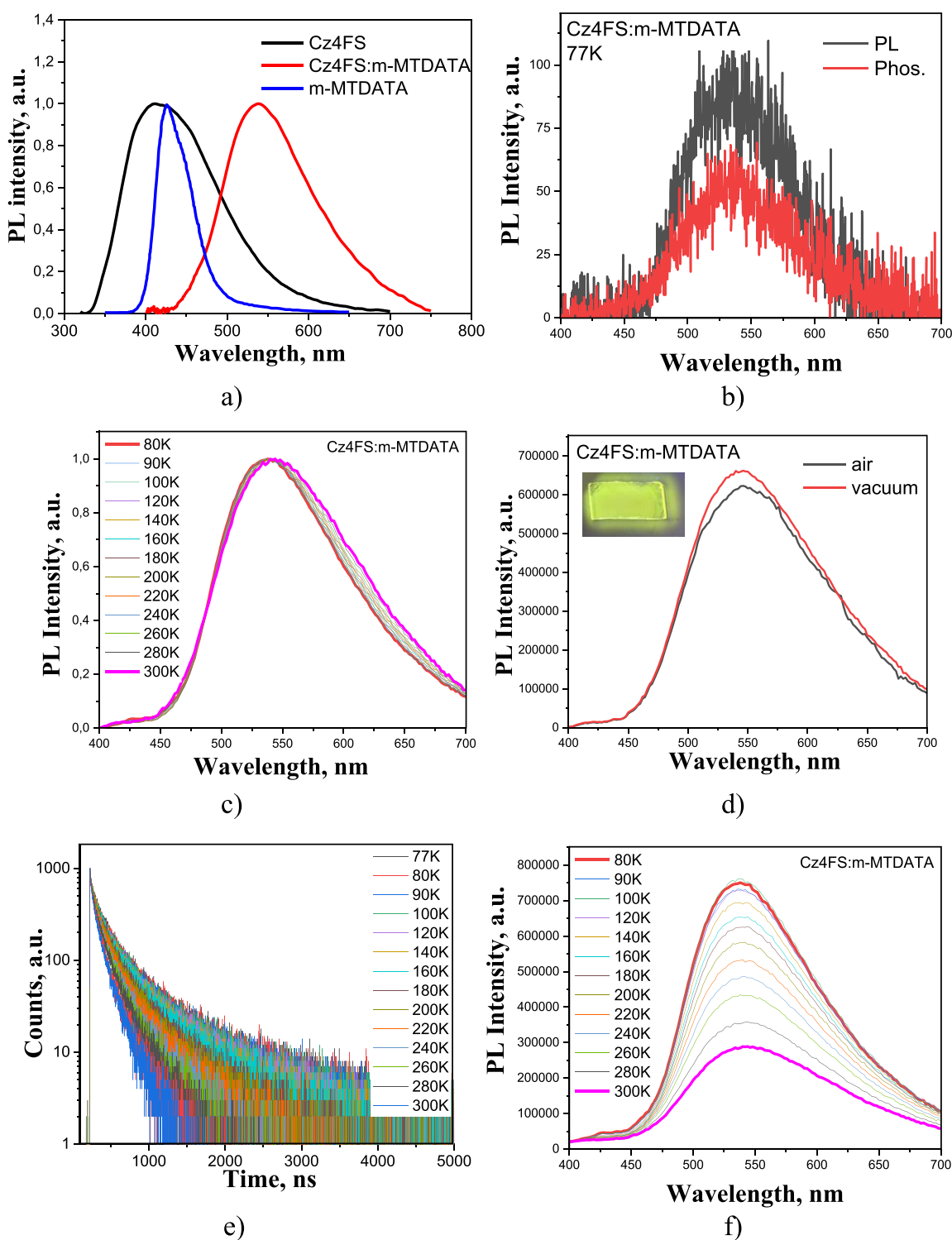
Figure 3. PL spectra (a) of vacuum-deposited films of m-MTDATA, Cz4FS, and the blend of Cz4FS and m-MTDATA. PL and phosphorescence spectra at 77 K (b), normalized PL spectra (c) at different temperatures, PL spectra (d) in air and vacuum (inset: photo of the tested sample in the air under UV excitation), PL decay curves (e), and PL spectra (f) at different temperatures of Cz4FS:m-MTDATA (50:50% by molar ratio). The excitation wavelength was 350 nm.

Non-normalized PL spectra of the investigated blends of mCP and Cz4FS with the different concentrations of Cz4FS as well as PL of the solid films of Cz4FS and mCP are depicted in Figure 1b. The PL intensity of Cz4FS increases and prevails over the weakened mCP peak as the emitter concentration grows. The molecular mixtures with the dopant concentration of 7% and 10% in the mCP host exhibited the highest PLQY

values of 15% and 17%, respectively (Table 1). Such concentration dependence means that efficient FRET takes place in the studied blends. Indeed, PLQY of the film of Cz4FS(10%) doped in mCP is very close to the PLQY of the pristine thin film of Cz4FS.

Compound Cz4FS is characterized by an ionization potential of 5.97 eV (related to the highest occupied molecular
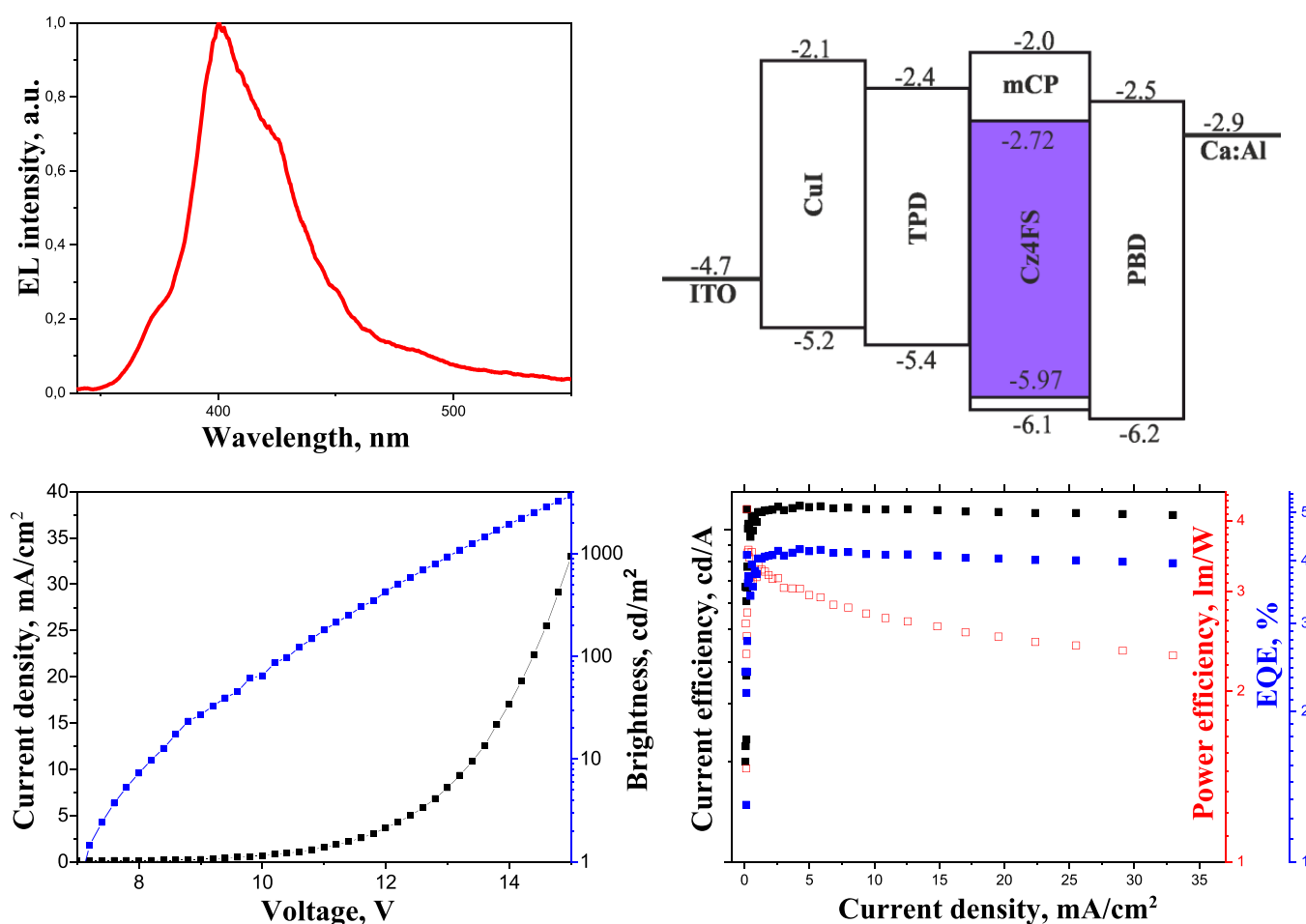
Figure 4. Energy level diagrams of device A and the corresponding normalized electroluminescence spectrum as well as brightness/current density−voltage and current efficiency/power efficiency/EQE-current density characteristics.

orbital (HOMO) of −5.97 eV) and electron affinity of 2.72 eV (related to the lowest unoccupied molecular orbital (LUMO) of −2.72 eV). The value of the ionization potential (IP^{PE}) of Cz4FS was recorded by the photoelectron spectroscopy method in the air (Figure 2). The IP^{PE} value of Cz4FS agrees with its ionization potential (5.91 eV) previously measured by cyclic voltammetry.[35] The value of the electron affinity (EA^{PE}) of Cz4FS was calculated by the formula EA^{PE} = IP^{PE} − 1.37 × Eg^{opt},[41] where Eg^{opt} is the optical band gap (2.37 eV) taken from the low-energy onset of absorption spectra of the neat film of Cz4FS (Figure 1a). The different energy positions of the HOMO (−5.1 eV) and LUMO (−2 eV) are for 4,4′,4″-tris[(3-methyl phenyl)phenylamino]triphenylamine (m-MTDATA). Such HOMO−HOMO and LUMO−LUMO barriers of 0.87 and 0.72 eV between the donor m-MTDATA and acceptor Cz4FS provide the ability to form an exciplex exhibiting TADF (Figure 3a).

In addition, Cz4FS is characterized by a high triplet level of 3.0 eV, which is practically the same as that of mCP (Figure 1c,d). The triplets of Cz4FS and mCP were taken from high-energy edges of the corresponding phosphorescence spectra recorded at a delay of 50 ms after excitation (λ_{exc} = 300 nm). The high-efficient exciplexes are typically formed involving electron-donating and electron-accepting compounds with high triplets.[42]

Exciplexes are usually characterized by a small energy gap between the charge-transfer (CT) singlet and triplet (S$_1$, T$_1$)

states.[43] These states thus exist in thermal equilibrium due to the rapid processes of intersystem crossing (ISC) and reverse ICS at room temperature. Relaxation to the ground state occurs through the radiative S$_1$ → S$_0$ transition, and the corresponding long-living emission component is of TADF nature. This allowed us to reach an external quantum efficiency (EQE) for OLED-based Cz4FS doped in m-MTDATA higher than the 5% limit of the electrofluorescent devices.

The exciplex emission of the film of a molecular mixture of Cz4FS and m-MTDATA confirms the shift to the long-wavelength region of the spectrum of the photoluminescence relative to the corresponding spectra of the films of the neat compounds (Figure 3a). In the case of the TADF exciplex, small singlet−singlet triplet splitting (ΔE_{ST}) is typically observed.[42] To check this requirement for the blend of Cz4FS and m-MTDATA, PL and phosphorescence spectra of Cz4FS:m-MTDATA were recorded at 77 K without and with a delay of 5 μs after excitation, respectively (Figure 3b). Due to the same high-energy edges of PL and phosphorescence spectra of Cz4FS:m-MTDATA, the ΔE_{ST} value is close to zero. This claim is in agreement with practically the same shapes of PL spectra of Cz4FS:m-MTDATA at different temperatures because of the similar shapes of PL and phosphorescence spectra (Figure 3c). In the case of TADF, the emission of the blend of Cz4FS and m-MTDATA should be sensitive to the presence of oxygen. The PL spectra of Cz4FS:m-MTDATA were recorded in air and vacuum (Figure 3d). The PL intensity
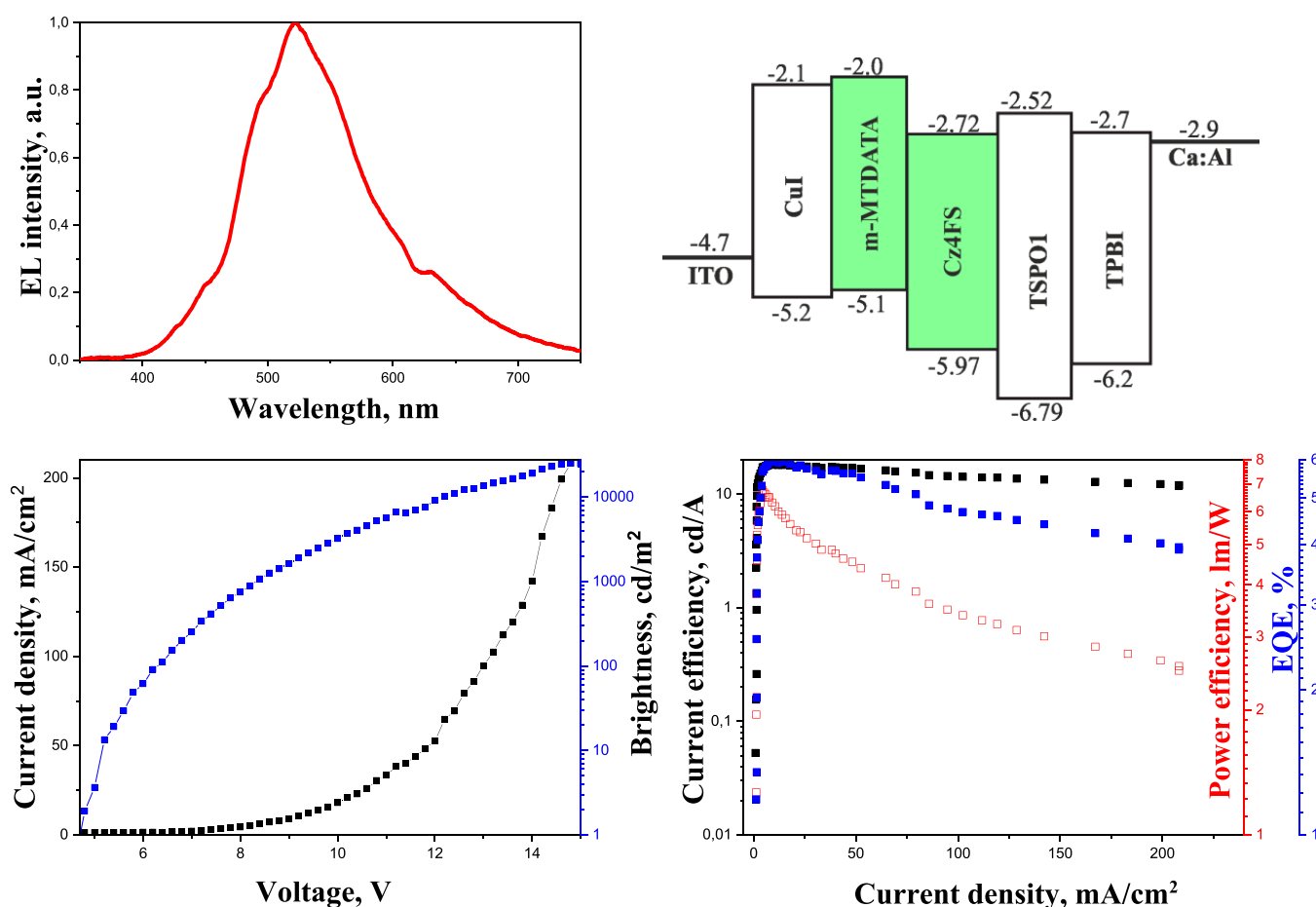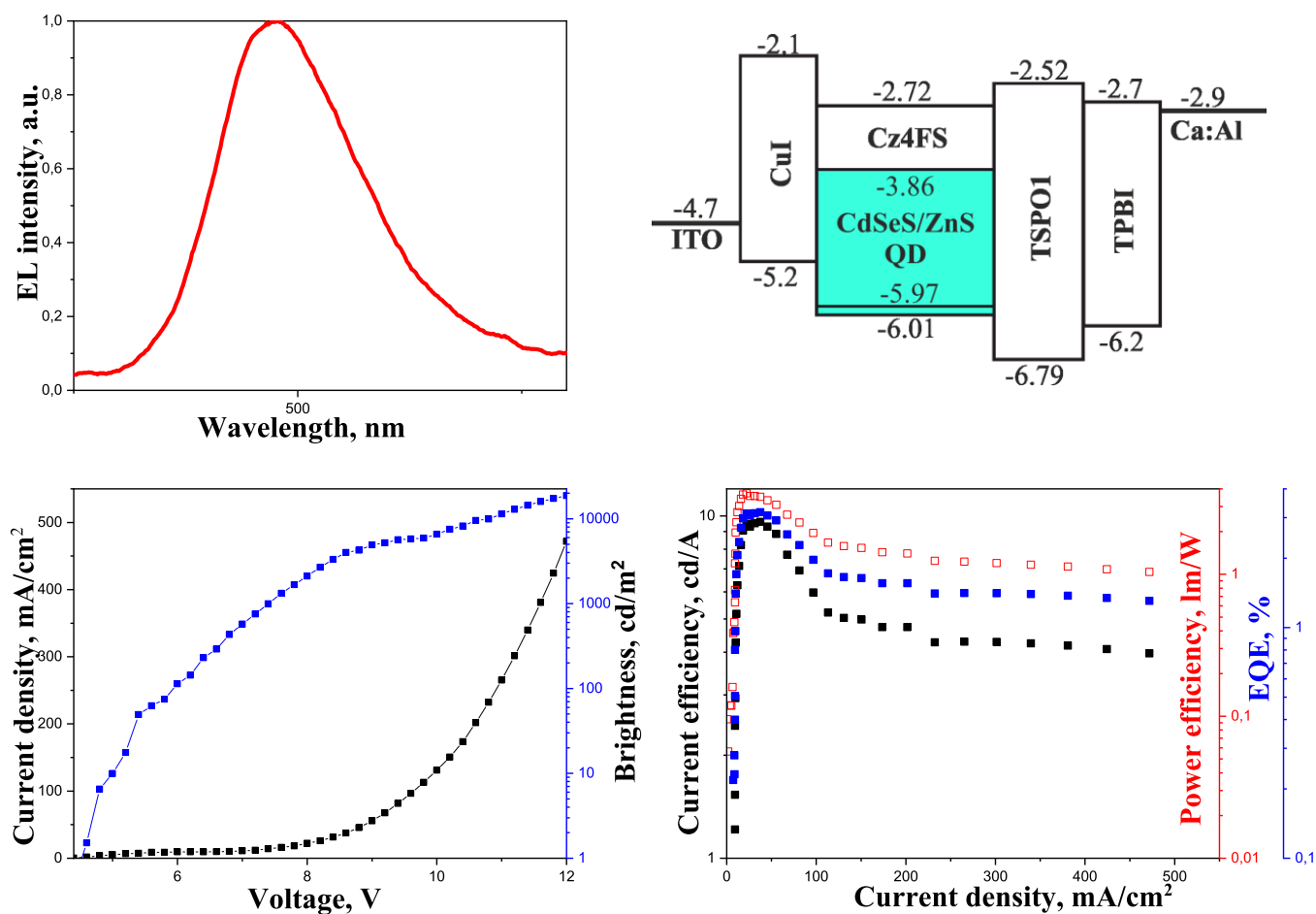
Figure 5. Energy level diagrams of device B and the corresponding normalized electroluminescence spectrum as well as brightness/current density−voltage and current efficiency/power efficiency/EQE-current density characteristics.

was slightly increased. Finally, the corresponding PL decay curves reached the range of milliseconds (Figure 3e). The long-living emission decay component of the film of the blend of Cz4FS and m-MTDATA confirms the TADF nature of photoluminescence. According to the biexponential fitting (χ^2 was 1.249), the PL decay curve of the film of the molecular mixture of Cz4FS and m-MTDATA is characterized by emission lifetimes τ_1 of 21.3 ns (44%) and τ_2 of 98.4 ns (56%) at room temperature. Such, long as for prompt fluorescence but short as for delayed fluorescence, emission lifetimes are not typical for conventional TADF exciplexes.[44,45] However, the emission lifetimes of the blend of Cz4FS and m-MTDATA are in very good agreement with that of a fast intersystem crossing assisted TADF exciplex or even hot exciplexes.[46,47] It should be noted that the PL intensity of Cz4FS:m-MTDATA decreases with increased temperature from 100 to 300 K (Figure 3e,f). A similar observation was previously published for a TADF exciplex due to the nonemissive energy loss.[48] Apparently, due to the nonemissive energy loss, the intensities of both delayed fluorescence (TADF) and phosphorescence of Cz4FS:m-MTDATA decrease with increased temperature.

Using poly(9-(2,3,5,6-tetrafluoro-4-vinylphenyl)-9H-carbazole) (**P1**)[35] and the copolymer of 9-(2,3,5,6-tetrafluoro-4-vinyl phenyl)-9H-carbazole and 9-(4-vinyl phenyl)carbazole (LRC-13), the polymer OLEDs were fabricated and studied. This idea was based on the promising thermal properties of these polymer materials, in particular, high glass transition

temperature T_g = 215 °C and high decomposition temperature T_d = 411 °C for **P1**.[35] They ensure the stability of the devices at high temperatures induced by high current densities.

Fabrication and Characterization of Host-Containing OLEDs. The electroluminescent properties of Cz4FS were studied using the conventional OLED structure based on the emitter doped into an mCP matrix. The device structure and the energy diagram are shown in Figure 4a. The general scheme of the fabricated OLED with the thicknesses of the layers was as follows: ITO/CuI(8 nm)/TPD(40 nm)/mCP:Cz4FS(20 nm,7%)/PBD(40 nm)/Ca(50 nm)/Al(200 nm) (device A). It was fabricated by step-by-step deposition of the hole- and electron-transport layers, co-deposition of the layer of the host and dopant, and deposition of metal electrodes onto a precleaned ITO-coated glass substrate under a vacuum of 10^{-5} Torr. ITO was used as an anode material. CuI and N,N'-bis(3-methyl phenyl)-N,N'-diphenyl benzidine (TPD) were used for the preparation of hole-transporting layers (HTL).[49] 2-(4-Biphenylyl)-5-phenyl-1,3,4-oxadiazole (PBD) was used for the deposition of the electron-transporting layer (ETL).[50] HTL and ETL were chosen for confining holes and electrons in the emitting layer, which helps to optimize OLED performance. The active area of the obtained devices was 6 mm². The layers of the guest−host system were formed by the method of thermovacuum co-deposition of mCP and Cz4FS with the concentration of the dopant Cz4FS (guest) of 7% by weight. It should be noted that mCP was chosen as the host material due to its high-lying

Figure 6. Energy level diagrams of device C and the corresponding normalized electroluminescence spectrum as well as brightness/current density−voltage and current efficiency/power efficiency/EQE-current density characteristics.

singlet excited state (3.6 eV) that matches well with the wide band gap blue light OLED emitters for efficient FRET.[51,52]

The luminance of device A was 10 cd/m² when a bias voltage of 7.4 V was applied to the organic heterostructure (Figure 4b). Although the onset voltage is considerable, but it is possible to reduce it by introducing additional electron- and hole-blocking layers. Device A demonstrated the best EL efficiency (4.2% (11.5 cd A⁻¹)) at a current density of 12.5 mA cm⁻². It should be noted that such values approach the theoretical maximum EQE limit of 5% expected for fluorescence-based OLEDs.[53] The current, power efficiency, and EQE characteristics of device A were stable in the wide range of current density values (Figure 4c). The maximum brightness of 3600 cd/m² was achieved at the voltage of 15 V.

The electroluminescence spectrum of device A (Figure 4b) was stable in a wide range of applied voltages. The spectral maximum for the OLED was at 413 nm. This observation is in good agreement with the wavelength of the PL intensity maximum of the film of the blend of mCP and Cz4FS (Figure 2). The OLED showed a narrow (fwhm of 45 nm) EL spectrum in the range from 387 to 432 nm (Figure 4b) without green emission with CIE coordinates (x = 0.15, y = 0.13), close to the deep blue color.

Fabrication and Characterization of an Exciplex OLED. The electroluminescent properties of device B based on exciplex emission of the blend of Cz4FS and mMTDATA were studied using the following OLED architecture: ITO/

CuI(8 nm)/m-MTDATA(20 nm):Cz4FS(20 nm)/TSPO1(10 nm)/TPBI(30 nm)/Ca (50 nm)/Al(200 nm). The energy diagram of device B is presented in Figure 5. The layer of m-MTDATA had a dual function in device B. m-MTDATA served as an efficient HTL material, as well as a donor component of the exciplex-emitting blend. Accordingly, Cz4FS served as an acceptor of the exciplex-forming molecular mixture. Diphenylphosphine oxide-4-(triphenylsilyl)phenyl (TSPO1) was used as an electron-blocking (EBL) material. 2,2″,2′-(1,3,5-Benzinitriyl)-tris(1-phenyl-1H-benzimidazole) (TPBi) was used for the preparation of an ETL layer supplying electrons from the Ca:Al cathode into the active area of device B. It should be noted that deposition of donor and acceptor components of the exciplex-forming blend was carried simultaneously from two crucibles with a mass ratio of components of 1:1.

Electrons injected from the cathode overcome the energy barrier of 0.42 eV when drifting from the LUMO level of Cz4FS (acceptor) to the LUMO level in m-MTDATA (Figure 5a). The barrier for holes injected from the HOMO level of m-MTDATA (donor) to the HOMO level of Cz4FS is 1 eV. Electrons and holes are thus accumulated in the blend of Cz4FS and m-MTDATA due to the presence of such high energy barriers. As a result, the cross-coupling of electrons at the LUMO of Cz4FS and holes at the HOMO of m-MTDATA is implemented, and the corresponding charge-transfer states are responsible for electroluminescence of device B.
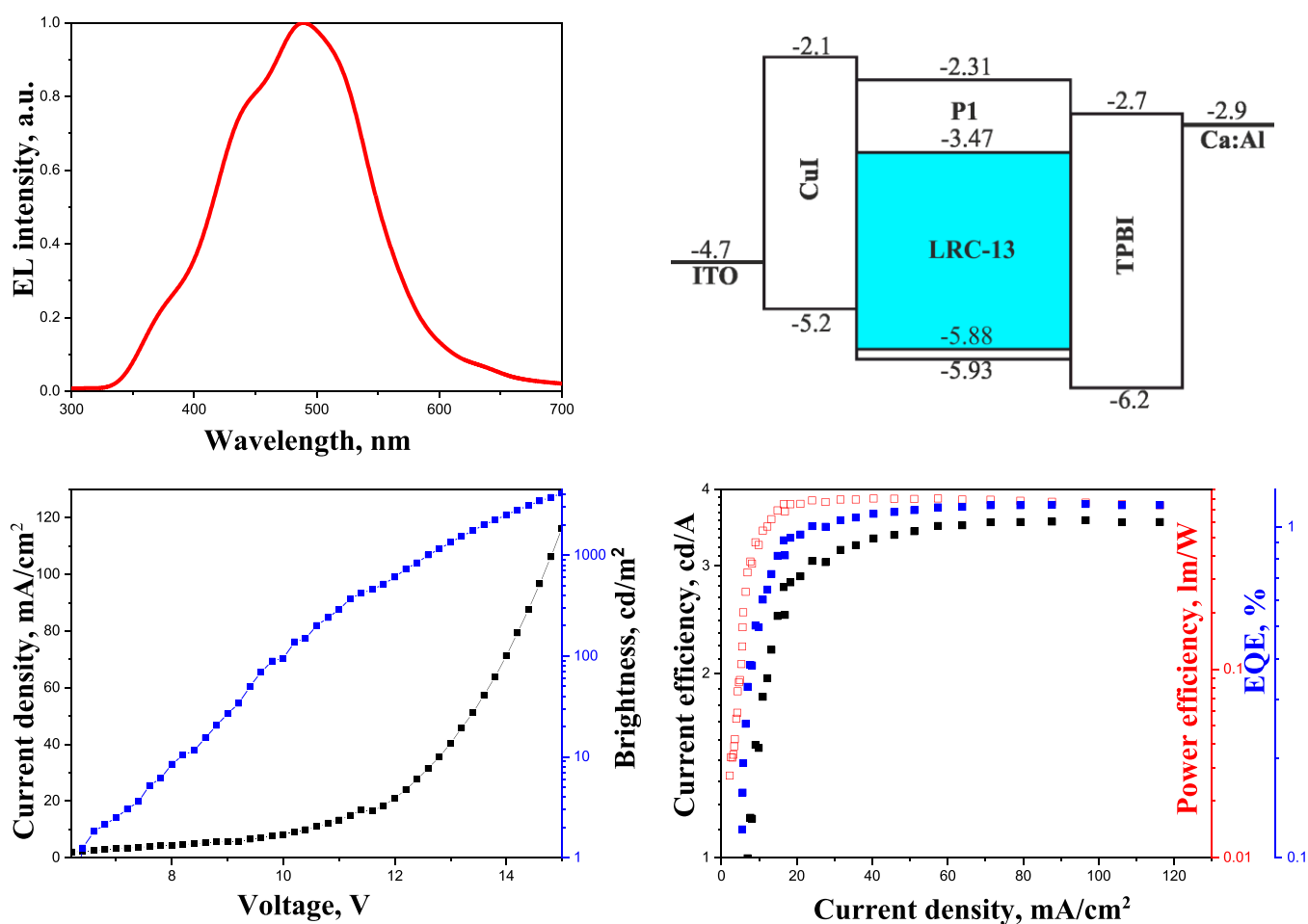
Figure 7. Energy level diagrams of device D and the corresponding normalized electroluminescence spectrum as well as brightness/current density−voltage and current efficiency/power efficiency/EQE-current density characteristics.

Table 2. Characteristics of OLED Devices A−D

device	V_{on}, V	brightness, cd/m²	current efficiency, cd/A	power efficiency, Lm/W	EQE, %	current efficiency, cd/A	power efficiency, Lm/W	EQE, %
			max				at 1000 cd/m²	
A	6.8	3600	11.5	3.8	4.2	10.5	2.3	3.9
B	4.7	24 700	12.0	6.8	5.3	17.6	6.6	5.8
C	4.5	18 700	9.6	4.6	2.3	4.1	1.1	1.3
D	6.0	4100	3.5	0.74	1.4	3.4	0.73	1.4

The weak shoulder near 450 nm in the electroluminescence spectrum of device B corresponds to pure exciton emission of m-MTDATA (Figure 5b). The rest of the EL spectrum of device B with a maximum around 520 nm clearly matches with the photoluminescence spectrum of the film of the molecular mixture of Cz4FS and m-MTDATA (Figure 3). The stable EL spectra indicate the absence of conformational disorder effects that could occur under different driving voltages.

The brightness of device B of 10 cd/m² at the bias voltage of 4.2 V was observed. The OLED was characterized by an EQE of 5.3%, slightly beyond the theoretical limit for fluorescent OLEDs. Similarly to device A, the EQE and power efficiency of device B showed relatively stable characteristics in a wide range of current density values (Figure 5c (inset)). The maximum value of the current efficiency of 12 cd/A and the maximum brightness of 24 700 cd/m² was achieved at an applied voltage of 15 V (Figure 5c). The CIE coordinates ($x = 0.22$, $y = 0.46$) of the device were also quite stable under the different voltages.

Fabrication and Characterization of the QLED. A quantum dot (QD)-based LED (named as QLED or device C) was of the following structure (Figure 6a): ITO/CuI(8 nm)/Cz4FS:CdSeS/ZnS(wt %,QD = 15%)(40 nm)/TSPO1(10 nm)/TPBI(40 nm)/Ca/Al. CuI[54] and TPBI[55] were used as materials for the HTL and ETL, respectively. The hole-blocking layer of TSPO1[56] and the Ca/Al cathode were consecutively evaporated in a vacuum chamber under 10^{-5} Torr. The host material Cz4FS and CdSeS/ZnS QDs were dispersed in toluene in the proportion of 1 mg per 1 mL. A solution with a concentration of 15% of the emitter and of 85% of the matrix was prepared. The layer of the mixture of Cz4FS and CdSeS/ZnSCdSeS/ZnS was casted from the dispersion in toluene to the surface of the ITO substrate with the preformed CuI film by centrifugation at 1000 rpm, followed by annealing at the temperature of 50 °C.

The developed QLED architecture is suitable for accumulation of electron−hole pairs in the active layer of the mixture
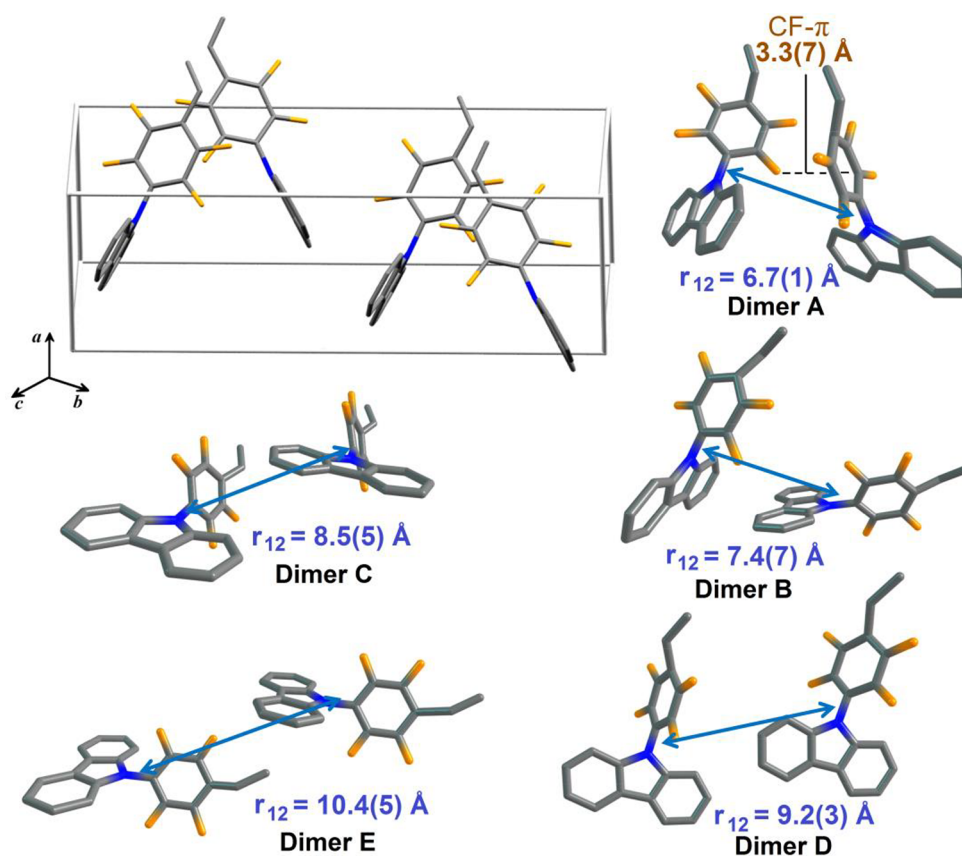
Figure 8. Pertinent dimers extracted from the crystal structure of Cz4FS. The intermolecular center-to-center (r_{12}) distances are shown by blue arrows. Hydrogen atoms are omitted for clarity.

Table 3. Center-to-Center Distances, Reorganization Energies, Transfer Integrals, Rates of Charge Hopping, and Charge Transfer Mobilities of Cz4FS Calculated at the B3LYP/TZP Theory Level

| compound	type of dimer	r_{12} (Å)	reorganization energy (meV)		transfer integral (V, meV)		rate of charge hopping (k, s^{-1})		charge transfer mobility, μ	
			hole	electron	hole	electron	hole	electron	hole	electron
1	A	6.714	128	431	−2.94	57.75	1.17×10^{11}	1.29×10^{12}	0.407	0.035
	B	7.469			25.73	−3.84	8.95×10^{12}	5.70×10^{9}		
	C	8.551			−17.78	12.03	4.27×10^{12}	5.59×10^{10}		
	D	9.230			−8.64	4.35	1.01×10^{12}	7.32×10^{9}		
	E	10.446			1.30	2.58	2.29×10^{10}	2.57×10^{9}		

of Cz4FS and CdSeS/ZnS (Figure 6a). It is due to the insignificant energy barrier (0.1 eV) between the LUMO energy level of the host material and the electron-transporting material (TSPO1) and the deep HOMO level of TSPO1 of ca. 6.79 eV, which facilitates the injection of electrons of the host material and makes it difficult to transport holes to the cathode. The main reason for the selection of CuI as the hole-injection layers is its valence band of −5.2 eV,[57] high conductivity ranging between 0.01 and 1 S/cm, and the high hole mobility of 20 cm^2 V^{-1} s^{-1}.[58,59]

The current density–voltage and voltage–luminance curves of the QLED are shown in Figure 6c. Device C shows the maximum luminance of 18 700 cd/m^2 at 12 V (Figure 6c). The chromaticity coordinates of device C (x = 0.24, y = 0.37) coincide with those of PL of the CdSeS/ZnS quantum dots. The QLED showed a maximum EL intensity at 491 nm (Figure 6b). The maximum EQE value of ca. 2.3% of the QLED was observed in the range of current densities from 20

to 50 mA/cm^2 and slightly decreased to 1.08% at 100 mA/cm^2 (Figure 6c (inset)).

Fabrication and Characterization of the Polymer OLED. The polymer OLED (POLED) was fabricated using polymer P1 and copolymer LRC-13[36] as host and guest materials of the emissive layer, respectively. The structure of the POLED (device D) was as follows: ITO/CuI/P1:LRC-13(10 wt %)/TPBI/Ca/Al (Figure 7). The choice of P1 as the host was determined in particular by the presence of a carbazole fragment in the polymer. P1 is characterized by a wide optical band gap (3.62 eV) and HOMO and LUMO levels of 5.93 and 2.31 eV, respectively (Figure 7a).

Device D showed bright blue emission with an EL intensity maximum near 490 nm (Figure 7b), which is 45 nm red-shifted compared to the PL maximum of the film of LRC-13. However, the EL spectrum of device C and the PL spectrum of the LRC-13 film both are broad and cover almost the whole visible region. The dependences of current density and brightness on voltage are shown in Figure 7c. The device
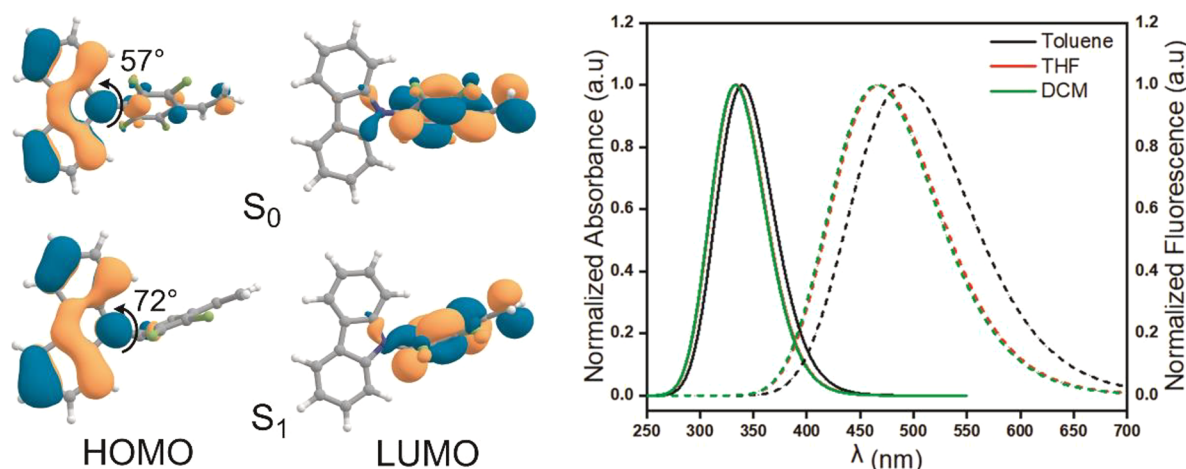
Figure 9. Shape of HOMO and LUMO orbitals of Cz4FS (isosurface control value 0.03 au) at ground (S_0) and excited (S_1) state geometries (left) and the simulated absorption and emission spectra (right).

Table 4. TD-DFT-PBE0/6-31G(d,p) Characterization of Absorption and Emission Properties of Cz4FS (Including Characterization of Electronic Energy Levels)[a]

solvent	λ^{abs}_{max}, nm	λ^{em}_{max}, nm	E(HOMO), eV	E(LUMO), eV	HLG, eV
toluene	328 ($f = 0.33$) [339]	438 ($f = 10^{-4}$) [490]	−5.67	−1.64	4.03
THF	328 ($f = 0.32$) [333]	456 ($f = 3 \times 10^{-4}$) [468]	−5.71	−1.62	4.09
DCM	328 ($f = 0.32$) [333]	456 ($f = 3 \times 10^{-4}$) [466]	−5.71 [−5.81]	−1.62 [−2.41]	4.09 [3.40]

[a]Experimental values are presented in brackets; oscillator strengths for the corresponding S_0−S_1 and S_1−S_0 vertical transitions are presented in parentheses.

reached a maximum brightness of 4100 cd/m^2 and EQE$_{max}$ of 1.4% (Figure 7c (inset)). The developed POLED had excellent low efficiency roll-off in a wide range of current density values. Stable EL spectra of the device for different bias voltages were also recorded (Figure S1), which indicates the absence of the conformational disorder effects in electroluminescence of device D. The CIE coordinates of the emission of the POLED were also stable under different control voltages and were estimated as ($x = 0.22$, $y = 0.31$). Comparing the dependence of EL parameters on the applied current density of device A to device D, one can see that the latter has voltage-indifferent EL behavior, while device A demonstrates some slight degradation with increasing current density. The key parameters of devices A−D measured at the same conditions are given in Table 2.

Computational Study. To further investigate the properties of Cz4FS, we have studied its electron/hole mobilities computationally. We suggest that the reason that this compound demonstrates multifunctional behavior as a component of different types of OLEDs is that it possesses stable luminescence characteristics combined with ambipolar conductivity. Thus, starting from the crystal structure, we have studied the carrier hopping pathways of Cz4FS within five intermolecular packing modes denoted as A−E (Figure 8, Table 3).

The main pathway for hole-transport corresponds to the face-to-edge B-dimer configuration. The hole-transport electronic coupling (V_{hole}) and related hopping rate (k_{hole}) for dimer B are significantly larger than those estimated for other dimers of compound Cz4FS, which indicates that the B packing mode is the dominant conducting channel for hole transport. The interesting observation is that dimer A represents the main pathway for electron transfer (in contrast

to hole mobility), and the corresponding electronic coupling is relatively high (58 meV, Table 3). The special feature of the A-dimer configuration is the presence of the stabilizing CF−π interaction with the distance of 3.37 Å due to the nearly perpendicular position of the C−F bond of one molecule of Cz4FS relative to the fluorinated aromatic ring of another molecule of Cz4FS.[60] The F−π interaction involves attraction between the partial negative charge on F atoms in one molecule and electropositive benzoic surface in another molecule. The dimer C demonstrates the equivalent coupling for hole and electron transport (Table 3) and complement hopping pathways within the other dimers A and B. The other dimers (D and E) sustain significantly longer intermolecular distances and much weaker electronic coupling that results in significantly lower hopping rates compared to those of dimers A−C (Table 3).

For Cz4FS the hole reorganization energy (λ_{hole}) is quite low (128 meV, Table 3), while the electron reorganization energy ($\lambda_{electron}$) is relatively large (431 meV, Table 3) because of the significantly distorted structure of its anionic state. As a result, the final hole mobility (μ_{hole}) is 1 order of magnitude larger (0.407 cm^2 V^{-1} s^{-1}) than the electron mobility ($\mu_{electron}$ = 0.035 cm^2 V^{-1} s^{-1}). However, accounting for the crystal restrictions, the distortion of anionic state structure might be suppressed, which usually leads to reduction of the reorganization energies.[61,62]

Absorption and emission properties of Cz4FS originate from its D−A structure that affects the CT nature of the S_1 state. In most cases, the CT nature of excited singlet states leads to a negligible intensity of the corresponding electronic transitions, but in the case of Cz4FS both HOMO and LUMO functions have nonzero contributions at the same atoms of D and A fragments when considering the ground-state (S_0) geometry

(Figure 9). The HOMO is delocalized not only on the donor carbazole fragment but also on the electron-accepting tetrafluorostyrene group, while the LUMO is mostly localized on the electron-accepting tetrafluorostyrene unit (Figure 9). The mutual rotation between D and A moieties for the S_0 state geometry is around 57°; that is, they are not fully orthogonal, and this allows some conjugation between the D and A units that results in the considerable intensity of S_0–S_1 absorption predicted at 328 nm (experimentally observed at 333–339 nm, Table 4) and insensitivity to the solvent polarity. In contrast, optimized S_1 state geometry is characterized by near-orthogonal mutual interposition (72°) of D and A moieties that results in negligibly small intensity of the S_1–S_0 emission. This finding is in agreement with the very small photo-luminescence quantum yield of the solution of Cz4FS (9% for the solution in toluene).[35] However, in the solid film mutual rotation of D and A fragments is suppressed, and this results in a considerably higher photoluminescence quantum yield of 20%.[35]

As it follows from our computations, the structural changes upon excitation into the S_1 state do not change the orbital assignment of the S_1 excited state, and it corresponds to the HOMO–LUMO one-electron excitation. The computed energies of the HOMO and LUMO orbitals are in agreement with the experimental data (Table 4). The deviation in LUMO energies is quite significant such that is a known limitation of vertical DFT approximation.[63]

CONCLUSIONS

In this paper we report on the multifunctional applications of the simple donor–acceptor organic compound 9-(2,3,5,6-tetrafluoro-4-vinylphenyl)carbazole as the active and host material for emissive layers of organic light emitting devices. The polymer of Cz4FS and its copolymer with 9-(4-vinylphenyl)carbazole were also used as active components of OLEDs. We designed and characterized at least four types of OLEDs in which Cz4FS played the role of guest emitter (device A), the acceptor part of an exciplex emitter (device B), and host matrix for CdSeS/ZnS alloyed quantum dots used as an emitter (device C). In addition, the polymer of Cz4FS was used as a host, and its copolymer with 9-(4-vinylphenyl)-carbazole was used as guest of the emissive layer (device D). Devices A–D are characterized by common values of external quantum efficiency as for purely fluorescent OLEDs (up to the theoretical limit of 5%), but these devices sustain low-efficiency roll-off of electroluminescence in a wide range of current densities (this is particularly related to polymer device D). Compound Cz4FS has an intrinsic limitation of photo-luminescence efficiency because of the twisted charge-transfer nature of the fluorescent state geometry. This follows from the quantum-chemical calculations. Thus, prohibiting the mutual rotation of donor and acceptor fragments of Cz4FS by chemical tuning or by conformational restrictions taking place in the solid state is prioritized for the enhancement of luminescence quantum yield of Cz4FS and lighting character-istics of the devices utilizing Cz4FS as emitter.

ASSOCIATED CONTENT

Ⓢ Supporting Information

The Supporting Information is available free of charge at https://pubs.acs.org/doi/10.1021/acsaelm.3c00047.

Electroluminescence spectra of the devices at different applied voltages; details of theoretical calculations for charge carrier mobility (PDF)

AUTHOR INFORMATION

Corresponding Authors

Juozas Vidas Grazulevicius − *Department of Polymer Chemistry and Technology, Kaunas University of Technology, 51423 Kaunas, Lithuania;* ⓞ orcid.org/0000-0002-4408-9727; Email: juozas.grazulevicius@ktu.lt

Glib V. Baryshnikov − *Department of Chemistry and Nanomaterials Science, Bohdan Khmelnytsky National University, Cherkasy 18031, Ukraine; Laboratory of Organic Electronics, Department of Science and Technology, Linköping University, Norrköping SE-60174, Sweden;* ⓞ orcid.org/0000-0002-0716-3385; Email: glib.baryshnikov@liu.se

Authors

Khrystyna Ivaniuk − *Lviv Polytechnic National University, 79013 Lviv, Ukraine*

Pavlo Stakhira − *Lviv Polytechnic National University, 79013 Lviv, Ukraine*

Iryna Yaremchuk − *Lviv Polytechnic National University, 79013 Lviv, Ukraine*

Stepan Kutsiy − *Lviv Polytechnic National University, 79013 Lviv, Ukraine*

Tetiana Bulavinets − *Lviv Polytechnic National University, 79013 Lviv, Ukraine*

Dmytro Volyniuk − *Department of Polymer Chemistry and Technology, Kaunas University of Technology, 51423 Kaunas, Lithuania;* ⓞ orcid.org/0000-0003-3526-2679

Ivan Klymenko − *Department of Polymer Chemistry and Technology, Kaunas University of Technology, 51423 Kaunas, Lithuania*

Galyna Sych − *University Grenoble Alpes, University Savoie Mont Blanc, CNRS, Grenoble INP, LEPMI, 38000 Grenoble, France*

Nataliya Karaush-Karmazin − *Department of Chemistry and Nanomaterials Science, Bohdan Khmelnytsky National University, Cherkasy 18031, Ukraine*

Amjad Ali − *Laboratory of Organic Electronics, Department of Science and Technology, Linköping University, Norrköping SE-60174, Sweden*

Aliaksei Vaitusionak − *Research Institute for Physical Chemical Problems of the Belarusian State University, 220006 Minsk, Belarus*

Sergei V. Kostjuk − *Research Institute for Physical Chemical Problems of the Belarusian State University, 220006 Minsk, Belarus;* ⓞ orcid.org/0000-0002-7466-3662

Complete contact information is available at:
https://pubs.acs.org/10.1021/acsaelm.3c00047

Notes

The authors declare no competing financial interest.

■ REFERENCES

(1) Guo, X.; Yuan, P.; Qiao, X.; Yang, D.; Dai, Y.; Sun, Q.; Qin, A.; Tang, B. Z.; Ma, D. Mechanistic Study on High-Efficiency Deep Blue AIE-Based Organic Light-Emitting Diodes by Magneto-Electroluminescence. *Adv. Funct. Mater.* **2020**, *30*, 1908704.

(2) Xu, R. P.; Li, Y. Q.; Tang, J. X. Recent advances in flexible organic light-emitting diodes. *J. Mater. Chem. C* **2016**, *4*, 9116−9142.

(3) Pode, R. Organic light emitting diode devices: An energy-efficient solid-state lighting for applications. *Renew. Sustain. Energy Rev.* **2020**, *133*, 110043.

(4) Amruth, C.; Pahlevani, M.; Welch, G. C. Organic light emitting diodes (OLEDs) with slot-die coated functional layers. *Mater. Adv.* **2021**, *2*, 628−645.

(5) Sun, J.; Ahn, H.; Kang, S.; Ko, S. B.; Song, D.; Um, H. A.; Kim, S.; Lee, Y.; Jeon, P.; Hwang, S.-H.; You, Y.; Chu, C.; Kim, S. Exceptionally stable blue phosphorescent organic light-emitting diodes. *Nat. Photon.* **2022**, *16*, 212−218.

(6) Li, Y.; Xu, Z.; Zhu, X.; Chen, B.; Wang, Z.; Xiao, B.; Lam, J. W. Y.; Zhao, Z.; Ma, D.; Tang, B. Z. Creation of efficient blue aggregation-induced emission luminous for high-performance non-doped blue OLEDs and hybrid white OLEDs. *ACS Appl. Mater. Interfaces* **2019**, *11*, 17592−17601.

(7) Sheats, J. R. Manufacturing and commercialization issues in organic electronics. *J. Mater. Res.* **2004**, *19*, 1974−1989.

(8) Yang, X.; Ding, L. Organic semiconductors: commercialization and market. *J. Semiconduct.* **2021**, *42*, 090201.

(9) Wu, Z.; Song, S.; Zhu, X.; Chen, H.; Chi, J.; Ma, D.; Zhao, Z.; Tang, B. Z. Highly efficient deep-blue fluorescent OLEDs based on anthracene derivatives with a triplet-triplet annihilation mechanism. *Mater. Chem. Front.* **2021**, *5*, 6978−6986.

(10) Jeong, M.; Joung, J. F.; Hwang, J.; Han, M.; Koh, C. W.; Choi, D. H.; Park, S. Deep learning for the development of organic optoelectronic devices: efficient prescreening of hosts and emitters in deep-blue fluorescent OLEDs. *npj Comp. Mater.* **2022**, *8*, 1−11.

(11) Wang, H.; Xie, L.; Peng, Q.; Meng, L.; Wang, Y.; Yi, Y.; Wang, P. Novel thermally activated delayed fluorescence materials−thioxanthone derivatives and their applications for highly efficient OLEDs. *Adv. Mater.* **2014**, *26*, 5198−5204.

(12) Yang, Z.; Mao, Z.; Xie, Z.; Zhang, Y.; Liu, S.; Zhao, J.; Xu, J.; Chi, Z.; Aldred, M. P. Recent advances in organic thermally activated delayed fluorescence materials. *Chem. Soc. Rev.* **2017**, *46*, 915−1016.

(13) Lee, J.; Chen, H. F.; Batagoda, T.; Coburn, C.; Djurovich, P. I.; Thompson, M. E.; Forrest, S. R. Deep blue phosphorescent organic light-emitting diodes with very high brightness and efficiency. *Nat. Mater.* **2016**, *15*, 92−98.

(14) Yook, K. S.; Lee, J. Y. Small molecule host materials for solution processed phosphorescent organic light-emitting diodes. *Adv. Mater.* **2014**, *26*, 4218−4233.

(15) Poriel, C.; Rault-Berthelot, J. Pure hydrocarbons: An efficient molecular design strategy for the next generation of host materials for Phosphorescent Organic Light-Emitting Diodes. *Acc. Mater. Res.* **2022**, *3*, 379−390.

(16) Ji, L.; Shi, J.; Wei, J.; Yu, T.; Huang, W. Air-Stable Organic Radicals: New-Generation Materials for Flexible Electronics? *Adv. Mater.* **2020**, *32*, 1908015.

(17) Lee, J. H.; Jeong, C. H.; Godumala, M.; Kim, C. Y.; Kim, H. J.; Hwang, J. H.; Kim, Y. W.; Choi, D. H.; Cho, M. J.; Choi, D. H. Rational design, synthesis, and characterization of a photocrosslink-

able hole-transporting polymer for high-performance solution-processed thermally activated delayed fluorescence OLEDs. *J. Mater. Chem. C* **2020**, *8*, 4572−4579.

(18) Monkman, A. Why Do We Still Need a Stable Long-Lifetime Deep Blue OLED Emitter? *ACS Appl. Mater. Interfaces.* **2022**, *14*, 20463−20467.

(19) Chan, C. Y.; Cui, L. S.; Kim, J. U.; Nakanotani, H.; Adachi, C. Rational molecular design for deep-blue thermally activated delayed fluorescence emitters. *Adv. Funct. Mater.* **2018**, *28*, 1706023.

(20) Liu, X.; Li, J.; Qiu, X.; Ye, X.; Xu, L.; Hu, D. Highly efficient non-doped deep-blue OLED with NTSC CIEy and negligible efficiency roll-off based on emitter possessing hydrogen bond and hybridized excited state. *Dyes Pigm.* **2022**, *200*, 110135.

(21) Chen, S.; Lian, J.; Wang, W.; Jiang, Y.; Wang, X.; Chen, S.; Zeng, P.; Peng, Z. Efficient deep blue electroluminescence with CIE y∈(0.05−0.07) from phenanthroimidazole−acridine derivative hybrid fluorophores. *J. Mater. Chem. C* **2018**, *6*, 9363−9373.

(22) Li, W.; Chasing, P.; Nalaoh, P.; Chawanpunyawat, T.; Chantanop, N.; Sukpattanacharoen, C.; Kungwan, N.; Wongkaew, P.; Sudyoadsuk, T.; Promarak, V. Deep-blue high-efficiency triplet-triplet annihilation organic light-emitting diodes using hydroxyl-substituted tetraphenylimidazole-functionalized anthracene fluorescent emitters. *J. Mater. Chem. C* **2022**, *10*, 9968.

(23) Kang, S.; Lee, H.; Jung, H.; Jo, M.; Jung, M.; Park, J. Highly efficient chrysene emitters based on optimized side groups for deep blue emission. *Dyes Pigm.* **2018**, *156*, 299−306.

(24) Scholz, S.; Kondakov, D.; Lüssem, B.; Leo, K. Degradation Mechanisms and Reactions in Organic Light-Emitting Devices. *Chem. Rev.* **2015**, *115*, 8449−8503.

(25) Hladka, I.; Volyniuk, D.; Bezvikonnyi, O.; Kinzhybalo, V.; Bednarchuk, T. J.; Danyliv, Y.; Lytvyn, R.; Lazauskas, A.; Grazulevicius, J. V. Polymorphism of derivatives of tert-butyl substituted acridan and perfluorobiphenyl as sky-blue OLED emitters exhibiting aggregation induced thermally activated delayed fluorescence. *J. Mater. Chem. C* **2018**, *6*, 13179−13189.

(26) Kulhanek, J.; Bures, F.; Pytela, O.; Pippig, F.; Danko, M.; Mikysek, T.; Padelkova, Z.; Ludwig, M. Quadrupolar D-p-A-p-D chromophores with central tetrafluorobenzene acceptor and two peripheral N,N-dimethylamino and methoxy donors. *J. Fluor. Chem.* **2014**, *161*, 15−23.

(27) Lu, W.; Kuwabara, J.; Iijima, T.; Higashimura, H.; Hayashi, H.; Kanbara, T. Synthesis of π-Conjugated Polymers Containing Fluorinated Arylene Units via Direct Arylation: Efficient Synthetic Method of Materials for OLEDs. *Macromolecules* **2012**, *45*, 4128−4133.

(28) Thalladi, V. R.; Weiss, H.-C.; Bläser, D.; Boese, R.; Nangia, A.; Desiraju, G. R. C−H⋯F Interactions in the Crystal Structures of Some Fluorobenzenes. *J. Am. Chem. Soc.* **1998**, *120*, 8702−8710.

(29) Cho, Y. J.; Chin, B. D.; Jeon, S. K.; Lee, J. Y. 20% External Quantum Efficiency in Solution-Processed Blue Thermally Activated Delayed Fluorescent Devices. *Adv. Funct. Mater.* **2015**, *25*, 6786−6792.

(30) Greiner, R.; Schlücker, T.; Zgela, D.; Langhals, H. Fluorescent aryl naphthalene dicarboximides with large Stokes shifts and strong solvatochromism controlled by dynamics and molecular geometry. *J. Mater. Chem. C* **2016**, *4*, 1104−1110.

(31) Chen, W.; Chen, H.; Huang, Y.; Tan, Y.; Tan, C.; Xie, Y.; Yin, J. Molecular design and photothermal application of thienoisoindigo dyes with aggregation-induced emission. *ACS Appl. Bio Mater.* **2022**, *5*, 3428−3437.

(32) Luo, J.; Xie, Z.; Lam, J. W.; Cheng, L.; Chen, H.; Qiu, C.; Kwok, H. S.; Zhan, X.; Liu, Y.; Zhu, D.; Tang, B. Z. Aggregation-induced emission of 1-methyl-1, 2, 3, 4, 5-pentaphenylsilole. *Chem. Commun.* **2001**, *18*, 1740.

(33) Leung, N. L. C.; Xie, N.; Yuan, W.; Liu, Y.; Wu, Q.; Peng, Q.; Miao, Q.; Lam, J. W. Y.; Tang, B. Z. Restriction of Intramolecular Motions: The General Mechanism behind Aggregation-Induced Emission. *Chem.—Eur. J.* **2014**, *20*, 15349−15353.

(34) Liu, Y. Y.; Zhang, X.; Li, K.; Peng, Q. C.; Qin, Y. J.; Hou, H. W.; Zang, S. Q.; Tang, B. Z. Restriction of Intramolecular Vibration in Aggregation-Induced Emission Luminogens: Applications in Multifunctional Luminescent Metal−Organic Frameworks. *Angew. Chem., Int. Ed.* **2021**, *60*, 22417−22423.

(35) Sych, G.; Simokaitiene, J.; Lygaitis, R.; Jatautiene, E.; Pashazadeh, R.; Buika, G.; Grazulevicius, J. V. Structure-properties relationship of tetrafluoroethylene-based monomers and polymers containing different donor moieties. *React. Funct. Polym.* **2019**, *143*, 104323.

(36) Vaitusionak, A. A.; Vasilenko, I. V.; Sych, G.; Kashina, A. V.; Simokaitiene, J.; Grazulevicius, J. V.; Kostjuk, S. V. Atom-transfer radical homo- and copolymerization of carbazole-substituted styrene and perfluorostyrene. *Eur. Polym. J.* **2020**, *134*, 109843.

(37) Qin, W.; Shah, R. A.; Guyot-Sionnest, P. CdSeS/ZnS Alloyed Nanocrystal Lifetime and Blinking Studies under Electrochemical, Control. *ACS Nano* **2012**, *6*, 912−918.

(38) Deksnys, T.; Simokaitiene, J.; Keruckas, J.; Volyniuk, D.; Bezvikonnyi, O.; Cherpak, V.; Stakhira, P.; Ivaniuk, K.; Helzhynskyy, I.; Baryshnikov, G.; Minaev, B.; Grazulevicius, J. V. Synthesis and characterization of a carbazole-based bipolar exciplex-forming compound for efficient and color-tunable OLEDs. *New J. Chem.* **2017**, *41*, 559−568.

(39) Hladka, I.; Lytvyn, R.; Volyniuk, D.; Gudeika, D.; Grazulevicius, J. V. W-shaped bipolar derivatives of carbazole and oxadiazole with high triplet energies for electroluminescent devices. *Dyes Pigm.* **2018**, *149*, 812−821.

(40) Jeon, W. S.; Park, T. J.; Kim, S. Y.; Pode, R.; Jang, J.; Kwon, J. H. Ideal host and guest system in phosphorescent OLEDs. *Organ. Electron.* **2009**, *10*, 240−246.

(41) Sworakowski, J. How accurate are energies of HOMO and LUMO levels in small-molecule organic semiconductors determined from cyclic voltammetry or optical spectroscopy? *Synth. Met.* **2018**, *235*, 125−130.

(42) Sarma, M.; Wong, K.-T. Exciplex: An Intermolecular Charge-Transfer Approach for TADF. *ACS Appl. Mater. Interfaces* **2018**, *10*, 19279−19304.

(43) Zhang, M.; Zheng, C.-J.; Lin, H.; Tao, S.-L. Thermally activated delayed fluorescence exciplex emitters for high-performance organic light-emitting diodes. *Mater. Horiz.* **2021**, *8*, 401−425.

(44) Peng, J.; Xua, X.; Feng, X. J.; Li, L. Fabrication of solution-processed pure blue fluorescent OLED using exciplex host. *J. Luminesc.* **2018**, *198*, 19−23.

(45) Lin, T.-C.; Sarma, M.; Chen, Y.-T.; Liu, S.-H.; Lin, K.-T.; Chiang, P.-Y.; Chuang, W.-T.; Liu, Y.-C.; Hsu, H.-F.; Hung, W.-Y.; Tang, W.-C.; Wong, K.-T.; Chou, P.-T. Probe exciplex structure of highly efficient thermally activated delayed fluorescence organic light emitting diodes. *Nat. Commun.* **2018**, *9*, 3111.

(46) Traskovskis, K.; Sebris, A.; Novosjolova, I.; Turks, M.; Guzauskas, M.; Volyniuk, D.; Bezvikonnyi, O.; Grazulevicius, J. V.; Mishnev, A.; Grzibovskis, R.; Vembris, A. All-organic fast intersystem crossing assisted exciplexes exhibiting sub-microsecond thermally activated delayed fluorescence. *J. Mater. Chem. C* **2021**, *9*, 4532−4543.

(47) Schleper, A. L.; Goushi, K.; Bannwarth, C.; Haehnle, B.; Welscher, P. J.; Adachi, C.; Kuehne, A. J. C. Hot exciplexes in U-shaped TADF molecules with emission from locally excited states. *Nat. Commun.* **2021**, *12*, 6179.

(48) Kim, K.-H.; Yoo, S.-J.; Kim, J.-J. Boosting Triplet Harvest by Reducing Nonradiative Transition of Exciplex toward Fluorescent Organic Light-Emitting Diodes with 100% Internal Quantum Efficiency. *Chem. Mater.* **2016**, *28*, 1936−1941.

(49) Stakhira, P.; Cherpak, V.; Volynyuk, D.; Ivastchyshyn, F.; Hotra, Z.; Tataryn, V.; Luka, G. Characteristics of organic light emitting diodes with copper iodide as injection layer. *Thin Solid Films* **2010**, *518*, 7016−7018.

(50) Zhang, F.; Zhao, S.; Zhao, D.; Jiang, W.; Li, Y.; Yuan, G.; Zhu, H.; Xu, Z. Electroplex emission from bi-layer blue emitting organic materials. *Phys. Scr.* **2007**, *75*, 407.

(51) Yang, R. Y.; Li, X. M.; Cao, X. A. Role of wide bandgap host in the degradation of blue phosphorescent organic light-emitting diodes. *J. Appl. Phys.* **2017**, *122*, 075501.

(52) Vasilopoulou, M.; Yusoff, M.; Daboczi, M.; Conforto, J.; Gavim, A. E. X.; da Silva, W. J.; Macedo, A. G.; Soultati, A.; Pistolis, G.; Schneider, F. K.; Dong, Y.; Jacoutot, P.; Rotas, G.; Jang, J.; Vougioukalakis, G. C.; Chochos, C. L.; Kim, J.-S.; Gasparini, N. High-efficiency blue organic light-emitting diodes with below-bandgap electroluminescence. *Nat. Commun.* **2021**, *12*, 1−10.

(53) Chen, L.; Zhang, S.; Li, H.; Chen, R.; Jin, L.; Yuan, K.; Li, H.; Lu, P.; Yang, B.; Huang, W. Breaking the Efficiency Limit of Fluorescent OLEDs by Hybridized Local and Charge-Transfer Host Materials. *J. Phys. Chem. Lett.* **2018**, *9*, 5240−5245.

(54) Shan, M.; Jiang, H.; Guan, Y.; Sun, D.; Wang, Y.; Hua, J.; Wang, J. Enhanced hole injection in organic light-emitting diodes utilizing a copper iodide-doped hole injection layer. *RSC Adv.* **2017**, *7*, 13584.

(55) Liu, Z.; Zheng, W.; Wei, P.; Xu, Z.; Song, D.; Qiao, B.; Zhao, S. The improved performance and mechanism of solution-processed blue PhOLEDs based on double electron transport layers. *RSC Adv.* **2020**, *10*, 13215−13222.

(56) Sun, D.; Ren, Z.; Bryce, M. R.; Yan, S. Arylsilanes and siloxanes as optoelectronic materials for organic light-emitting diodes (OLEDs). *J. Mater. Chem. C* **2015**, *3*, 9496−9508.

(57) Konovalov, I.; Makhova, L. Valence band offset at interfaces between CuI and indium sulfides. *J. Appl. Phys.* **2008**, *103*, 103702.

(58) Inagaki, S.; Nakamura, M.; Aizawa, N.; Peng, L. C.; Yu, X. Z.; Tokura, Y.; Kawasaki, M. Molecular beam epitaxy of high-quality CuI thin films on a low temperature grown buffer layer. *Appl. Phys. Lett.* **2020**, *116*, 192105.

(59) Storm, P.; Bar, M. S.; Benndorf, G.; Selle, S.; Yang, C.; von Wenckstern, H.; Grundmann, M.; Lorenz, M. High mobility, highly transparent, smooth, p-type CuI thin films grown by pulsed laser deposition. *APL Mater.* **2020**, *8*, 091115.

(60) Li, P.; Maier, J. M.; Vik, E. C.; Yehl, Ch. J.; Dial, B. E.; Rickher, A. E.; Smith, M. D.; Pellechia, P. J.; Shimizu, K. D. Stabilizing Fluorine−π Interactions. *Angew. Chem., Int. Ed.* **2017**, *56*, 7209.

(61) Wu, Q.; Zhang, T.; Peng, Q.; Wang, D.; Shuai, Z. Aggregation induced blue-shifted emission − the molecular picture from a QM/MM study. *Phys. Chem. Chem. Phys.* **2014**, *16*, 5545−5552.

(62) Danyliv, Y.; Ivaniuk, K.; Danyliv, I.; Bezvikonnyi, O.; Volyniuk, D.; Galyna, S.; Lazauskas, A.; Skhirtladze, L.; Ågren, H.; Stakhira, P.; Karaush-Karmazin, N.; Ali, A.; Baryshnikov, G.; Grazulevicius, J. V. Carbazole-σ-sulfobenzimide derivative exhibiting mechanochromic thermally activated delayed fluorescence as emitter for flexible OLEDs: Theoretical and experimental insights. *Dyes Pigm.* **2022**, *208*, 110841.

(63) Zhang, G.; Musgrave, C. B. Comparison of DFT Methods for Molecular Orbital Eigenvalue Calculations. *J. Phys. Chem. A* **2007**, *111*, 1554−1561.